Graph-based Recurrence Quantification Analysis of EEG Spectral Dynamics for Motor Imagery-based BCIs

Sarah M. Ismail Hosni[1]*, Seyyed Bahram Borgheai[1], John McLinden[1], Shaotong Zhu[2], Xiaofei Huang[2], Sarah Ostadabbas[2], and Yalda Shahriari[1], *Member, IEEE*

Abstract— Despite continuous research, communication approaches based on brain-computer interfaces (BCIs) are not yet an efficient and reliable means that severely disabled patients can rely on. To date, most motor imagery (MI)-based BCI systems use conventional spectral analysis methods to extract discriminative features and classify the associated electroencephalogram (EEG)-based sensorimotor rhythms (SMR) dynamics that results in relatively low performance. In this study, we investigated the feasibility of using recurrence quantification analysis (RQA) and complex network theory graph-based feature extraction methods as a novel way to improve MI-BCIs performance. Rooted in chaos theory, these features explore the nonlinear dynamics underlying the MI neural responses as a new informative dimension in classifying MI. *Method:* EEG time series recorded from six healthy participants performing MI-Rest tasks were projected into multidimensional phase space trajectories in order to construct the corresponding recurrence plots (RPs). Eight nonlinear graph-based RQA features were extracted from the RPs then compared to the classical spectral features through a 5-fold nested cross-validation procedure for parameter optimization using a linear support vector machine (SVM) classifier. *Results:* Nonlinear graph-based RQA features were able to improve the average performance of MI-BCI by 5.8% as compared to the classical features. *Significance:* These findings suggest that RQA and complex network analysis could represent new informative dimensions for nonlinear characteristics of EEG signals in order to enhance the MI-BCI performance.

Keywords— Brain-computer interface (BCI), Nonlinear dynamics, Motor imagery (MI), Graph-based feature extraction, Recurrence quantification analysis (RQA).

I. INTRODUCTION

Motor imagery (MI)-based brain-computer interface (BCI) systems have the capacity to provide an innovative alternative neural communication channel for patients suffering from severe neuromuscular disabilities such as amyotrophic lateral sclerosis (ALS), cerebral palsy, spinal cord injury, and stroke patients [1], [2]. Enhancing the performance of these systems depends crucially on improving the classification of the sensorimotor rhythms (SMR), including μ (8–12 Hz) and β (13–25 Hz) frequency band modulations during MI tasks. MI-BCIs primarily rely on classifying the oscillatory variations in the μ and β frequency bands, known as event-related desynchronization (ERD) and event-related synchronization (ERS) [3]. Spectral analysis methods such as wavelet transforms, Fourier transforms, and autoregressive models have always been considered the traditional analysis methods for detecting MI patterns in MI-BCIs [4]. Despite continuous research efforts, EEG-based BCIs attain far from satisfactory performance levels. This is partially due to the inherent complex nonstationary nature of EEG, and to potential disease-specific abnormalities in patient's electrical responses which impose additional challenges to the extraction of discriminative features from their MI responses [2], [5]. Novel analysis methods of MI-based EEG responses are required for the progress of the BCI field to fully exploit the underlying neural dynamics embedded in these complex signals and translate them meaningfully into an efficient means of communication. Recurrence quantification analysis (RQA) has been successfully applied as a powerful nonlinear analysis tool to measure the complexity of numerous biological signals, especially when traditional techniques fail. Due to RQA's suitability for the analysis of short, noisy and nonstationary time series, in [6] RQA complexity measures were proposed as a new way to analyze event-related potentials by identifying transitions in the brain process during surprising moments on a single trial level as opposed to the traditional averaging of many trials, emphasizing the robustness of the RQA. Pitsik et al. [7] applied RQA to extract features, namely determinism (DET) and recurrence time entropy (RTE), to measure the reduction of EEG complexity during motor execution (ME) tasks. The extracted features were sensitive to the transitions from Rest to ME, suggesting the potential application of RQA to BCIs. However, their results were not accompanied by an evaluation of classification performance. Moreover, despite the overlap in the induced neural responses of MI and ME tasks [3], the complexity patterns identified for ME responses need to be verified for MI tasks for a practical MI-BCI system that can potentially be used by patients who have lost their voluntary muscle control and are unable to do any ME task.

The aim of this study is to analyze the nonlinear dynamics and recurrence patterns underlying the MI-based EEG neural responses using RQA and complex network theory. Eight nonlinear graph-based RQA features were extracted from the recurrence plots (RPs) reconstructed from each one-dimensional EEG time series measured at each channel and its adjacency matrix reinterpretation. EEG data were recorded from six healthy participants performing a MI-Rest task. Changes in the recurrence dynamics between MI and Rest quantified using these nonlinear features were evaluated and compared to classical linear spectral features to investigate their use as a new feature extraction method towards improving the performance of existing MI-BCI systems. The

[1]Sarah M. Ismail Hosni*, Seyyed Bahram Borgheai, John McLinden, and Yalda Shahriari are with the Department of Electrical, Computer and Biomedical Engineering, University of Rhode Island (URI), Kingston, RI 02881 USA (*Corresponding author's e-mail: sarah_hosni@uri.edu).
[2]Shaotong Zhu, Xiaofei Huang, and Sarah Ostadabbas are with the Department of Electrical and Computer Engineering, Northeastern University, Boston, MA 02115 USA.

performance was evaluated through a 5-fold cross-validation procedure using a linear support vector machine (SVM). The proposed analyses offer a new informative dimension in decoding MI neural signatures and discriminating it from Rest tasks for a MI-based BCI application which conventionally rely on linear spectral methods.

II. METHODS

A. Data Acquisition, Participants and Experimental Protocol

EEG signals were recorded from 13 Ag/AgCl electrodes referenced to the left earlobe and amplified using a g.USBamp amplifier (g.tec medical engineering). The signals were digitized at 256 Hz and zero-phase bandpass filtered 1–45 Hz. The EEG electrodes covered the pre-motor (FC3, FC4), primary motor (C1, C3, Cz, C2, C4), sensorimotor (CP1, CP3, CP2, CP4), and parietal (P3, P4) areas of the brain according to the 10–20 system. Data acquisition and the design of the MI paradigm were handled by BCI2000 software [8]. Six healthy participants with no reported history of neurological disease attended two MI data recording sessions on separate days. The data recording was performed in the NeuralPC Lab, University of Rhode Island (URI) with Institutional Review Board (IRB) approval. Each session contained three runs, and each run consisted of 40 trials of MI task or Rest (20 trials each) based on a visual on-screen queue. The MI task involved imagining the left- or right-hand movement, and each MI trial was followed by a Rest trial. Each trial lasted for 10 seconds. None of the participants had previous BCI experience. The first session was used to familiarize the subjects with the task and the second session was used for data analysis.

B. Data Preprocessing

The data were re-referenced offline using a common average reference (CAR) [9]. Eye movement artifacts were removed using the extended Infomax Independent Component Analysis (ICA) algorithm [10]. The artifact-free EEG signal was then reconstructed after removing the predominant artifactual components identified by visual inspection. The data were then zero-phase bandpass filtered into the μ (8–12 Hz) and β (13–25 Hz) frequency bands for further analysis. The data were segmented into 10-sec trials synchronized with the appearance of the visual stimulus cues (Rest/LMI/RMI). For MI vs. Rest classification, trials were combined to form two sets with 60 trials for each condition of MI and Rest representing the two classes. Individual MI tasks that contained artifacts were automatically rejected based on subject-specific thresholds. For the classical linear spectral features, the average power spectral density (PSD) was calculated using the Welch method from the filtered EEG signals giving PSD_μ and PSD_β extracted from each channel. This resulted into a total of 26 linear spectral features extracted from each trial from all the 13 EEG channels [11]. The features, within each frequency band, were extracted from an optimized response window that was performed for each subject in a nested 5-fold cross-validation classification procedure as explained in section E.

C. Recurrence Quantification Analysis (RQA)

In order to approximate the nonlinear neural dynamics underlying the MI and Rest tasks within the μ and β frequency bands separately, the bandpass filtered one-dimensional EEG signal measured at each frequency band, each channel, and each trial was projected to a multi-dimensional phase space based on Takens' theorem of time-delay embedding [12] using the following equation [13]:

$$X_k = (x_k, x_{k+\tau}, \dots, x_{k+(m-1)\tau}) \qquad (1)$$

where X_k is the reconstructed phase space vector based on the observation x_k of the bandpass filtered EEG time series $(x_1, x_2, \dots, x_L)$, τ is the time delay, m is the embedding dimension, and L is number of samples in the EEG time series. The time-delay parameter τ and the embedding dimension m were estimated using the average mutual information (AMI) and the false nearest neighbor (FNN) methods respectively [14]. These parameters were calculated for each participant using only the training set in the 5-fold cross-validation procedure as explained in section E. The phase space reconstruction can be represented as an N x m trajectory matrix $X = (X_1, X_2, \dots, X_N)$ where $N = L - (m - 1)$ is the number of states. Then, the recurrence plots (RPs) were created to visualize and quantify the recurrence patterns of the m-dimensional phase space trajectory X corresponding to each trial within each frequency band in a 2-dimensional plot [14]. RPs were constructed by considering an ε-neighborhood of states in phase space using the following equation:

$$RP_{i,j}(\varepsilon) = \Theta(\varepsilon - \|X_i - X_j\|) \quad i,j = 1, \dots, N \qquad (2)$$

where RP is the N x N recurrence plot, N is the number of states in time, Θ is the Heaviside function, ε is the recurrence threshold determining the size of the neighborhood in state space, $\|\blacksquare\|$ is the Euclidean norm, and X is the reconstructed phase space vector. The recurrence exists when $RP_{i,j}=1$, (i.e., when the state space vectors at time i and j are within the same ε-neighborhood). The choice of the ε-neighborhood threshold was based on previous studies' recommendation that it should not exceed 10% of the maximum phase space diameter [12]. Therefore, the value of ε was optimized for each participant by choosing from four different thresholds, namely 3%, 5%, 7%, and 10% of the maximum phase space diameter within the nested cross-validation classification procedure explained in section E. As it is common to find small distances between points in the reconstructed phase space that are close in time, the Theiler window in this study was set to a value of $(m - 1)\tau$ so that only points that are farther than $(m - 1)\tau$ from the diagonal were taken into account in the evaluation of the RQA measures according to [15].

Eight nonlinear graph-based RQA features were extracted from the recurrence plots (RPs) reconstructed from each one-dimensional EEG time series measured at each channel. The features were: recurrence rate (RR), determinism (DET), maximum length of diagonal lines (LMAX), laminarity (LAM), maximum length of vertical lines (VMAX), and recurrence time entropy (RTE), extracted in order to quantify the vertical and diagonal line structures in the reconstructed RPs of each trial. In addition, to include the topological characteristics of the recurrence patterns, two features from complex network theory, namely the global clustering coefficient (CC) and transitivity (T) were

extracted from the adjacency matrix reinterpretation of the RP. The features were extracted from the RP corresponding with μ and β frequency bands separately using the following equations [16]:

$$RR = \frac{100}{N^2} \sum_{i,j=1}^{N} RP_{i,j} \qquad (3)$$

where RR is the recurrence rate, which is a measure of the density of recurrence points in the RP, N is the number of states.

$$DET = \frac{\sum_{l=l_{min}}^{N} lP(l)}{\sum_{l=1}^{N} lP(l)} \qquad (4)$$

where DET is a relative measure of the system's regularity, defined as the percentage of recurrence points forming diagonal structures with respect to all recurrence points in RP. $P(l)$ is distribution of diagonal lines of length l, and $l_{min} = 2$ is the length of the shortest diagonal [12].

$$LMAX = \max(\{l_i : i = 1 \dots N_l\}) \qquad (5)$$

where $LMAX$ is the maximum length of diagonal structures, l_i is the length of diagonal line i, and N_l is the total number of diagonal lines.

$$LAM = \frac{\sum_{v=v_{min}}^{N} vP(v)}{\sum_{v=1}^{N} vP(v)} \qquad (6)$$

where LAM is the laminarity, representing the probability of occurrence of laminar states in the system, $P(v)$ is the distribution of vertical lines of length v, and $v_{min} = 2$ [6].

$$VMAX = \max(\{v_i : i = 1 \dots N_v\}) \qquad (7)$$

where $VMAX$ is the maximum length of vertical structures, i.e., the longest duration of the laminar states, v_i is the length of vertical line i, and N_v is the total number of vertical lines.

$$RTE = - \sum_{t_w=1}^{T_{max}} p(t_w) \ln p(t_w) \qquad (8)$$

where RTE is the recurrence time enropy, i.e., the entropy of the "white" (non-recurrent) vertical lines indicating recurrence times t_w. $p(t_w) = P(t_w)/N_w$ is the estimated probability of a recurrence time t_w and $P(t_w)$ is distribution of recurrence times [7].

To extract the topological characteristics of the trajectory in phase space, the RP was reinterpreted as a binary adjacency matrix of undirected, unweighted complex network [17]. Each node of the network corresponds to an EEG sample in time, and edges are conveniently represented by the recurrence links, based on the ε-neighborhood in phase space [18]. The relationship between the RP and the corresponding adjacency matrix A is as follows:

$$A_{i,j} = RP_{i,j} - \delta_{i,j} \qquad (9)$$

where $\delta_{i,j}$ is the Kronecker delta. $A_{i,j} = 1$ if vertex i connects to vertex j, and $A_{i,j} = 0$ if the edge (i,j) does not exist, i.e., there is no recurrence of the system's state at time i and j. Since in our study we considered a theiler window, the RP was regarded to be the adjacency matrix A for further analysis. From RP, two graph-based features were defined as follows [19]:

$$CC = \sum_{v=1}^{N} \frac{C_v}{N}. \qquad (10)$$

where CC is the global clustering coefficient introducing a new recurrence aspect of the RP as it represents the probability that two recurrences of any state are also neighbors, and C_v is the local clustering coefficient defined for each node v [19].

$$T = \frac{\sum_{i,j,k=1}^{N} A_{i,j} A_{j,k} A_{k,i}}{\sum_{i,j,k=1}^{N} A_{i,j} A_{k,i}} \qquad (11)$$

where T is transitivity, providing an effective measure for the global dimensionality of the underlying dynamical system [20].

In summary, a total of 208 nonlinear graph-based RQA features were extracted from each EEG trial from both μ and β frequency bands (i.e., eight features were extracted from each frequency band from each of the 13 channels) to quantify the nonlinear dynamics underlying the MI-Rest tasks. The features were extracted from optimized response windows within each frequency band for each subject through a nested cross-validation classification procedure as explained in section E.

D. Feature Selection

As the dimension of nonlinear features is relatively high, a feature selection scheme based on minimal Mahalanobis distance and maximal inter-feature correlation (mMMC) was adopted to exclude non-relevant and highly correlated features in order to avoid overfitting [21]. Moreover, mMMC was used to optimize the selection of the discriminative frequency band according to each subject's individual MI response as it was applied to the concatenated features from the μ and β frequency bands extracted using both the conventional spectral methods and the graph-based nonlinear RQA methods respectively. For this feature selection scheme, first, the features are sorted by their descending Mahalanobis distance, excluding those features that are lower than a defined threshold. Then, for the remaining features, the maximum Pearson correlation between that feature and the other features is determined and the feature is excluded if the value is above a certain correlation threshold. In this study, the Mahalanobis distance was set to 0.15, and the correlation threshold value was chosen from the interval of [0.84, 0.9] following previous studies [22].

E. Classification Procedure

Linear SVM, commonly used in MI-BCI, was used to evaluate the performance of each subject using a nested 5-fold cross-validation procedure to avoid biased estimation of the generalization error. To account for the high response variability in the neural data, the nonlinear RQA parameters as well as the classification parameters were estimated for each of the outer 5 cross-validation folds independently. The time delay τ and the embedding dimension m, were directly calculated using only the training set of each of the 5 cross-validation folds. The choice of the ε threshold was optimized among 3%, 5%, 7%, and 10% of the maximum phase space diameter thresholds using a nested 5-fold cross-validation procedure implemented as follows: for each of the outer 5 cross-validation folds, the training set was used to optimize the choice of ε based on the global peak of a nested 5-fold

cross-validation procedure. Hence, the optimized ε was estimated separately for each of the 5 outer cross-validation folds based only on the corresponding training set.

The response window was similarly optimized in the nested cross-validation inner-loop procedure for both the linear spectral features and the nonlinear graph-based RQA features. 2-sec, 5-sec, and 10-sec windows from each frequency band were considered for feature extraction and selection. For example, for a 10-sec window, features were extracted from the whole 10-sec trial bandpass filtered in the μ band and then concatenated with the features extracted from the 10-sec trial bandpass filtered in β band before the feature selection procedure. As each frequency band has its own separate dynamics, and with the β frequency band having higher frequency, the combinations of longer μ-band response windows with shorter β-band response windows were also considered resulting in a total of six possible response window optimizations to be considered in the nested cross-validation optimization. Due to the large number of nonlinear features (208 nonlinear graph-based RQA features for each trial), mMMC was applied to select the features extracted from each channel separately, as explained in section D, and the selected features from each channel were then concatenated for classification. For the linear features, mMMC was applied directly to the 26 features concatenated from all the channels. The performance was evaluated using 2 metrics: accuracy and F-score. The final optimized classification results are reported separately for each subject and averaged over all the 5 outer cross-validation folds.

III. RESULTS

Table I shows the optimized classification performance for each subject, comparing both the nonlinear RQA and graph-based feature extraction approach to the conventional linear PSD features. The table illustrates the optimized averaged 5-fold classification accuracy and the F-score for both feature extraction methods. As shown in this table the obtained average accuracies were 80.2%±6.5% and 74.4%±7.4% using nonlinear and linear features respectively.

For the linear PSD features, the optimized response window in the μ-band was 6.4±3.5 sec, 10.0±0.0 sec, 8.0±2.7 sec, 8.0±2.7 sec, 9.0±2.2 sec, and 5.2±4.4 sec for each subject respectively averaged across 5-fold cross-validation runs. For the β-band, the average optimized response window was 4.4±1.3 sec, 10.0±0.0 sec, 8.0±2.7 sec, 7.0±2.7 sec, 7.4±3.7 sec, and 5.2±4.4 sec for each subject respectively. The median number of selected linear PSD features was 15, 7, 11, 15, 13, and 4 for each subject respectively across all folds, and an average of 10.8±4.9 selected features across subjects.

TABLE I. OPTIMIZED CLASSIFICATION PERFORMANCE OF NONLINEAR RQA AND GRAPH-BASED FEATURES VS. LINEAR PSD SPECTRAL FEATURES

Participant No.	Nonlinear Features Accuracy (%)	Nonlinear Features F-score	Linear Features Accuracy (%)	Linear Features F-score
Subject-1	80.0	79.2	78.8	80.2
Subject-2	87.1	86.1	85.9	83.8
Subject-3	69.3	70.0	66.7	67.2
Subject-4	77.9	76.5	76.8	76.3
Subject-5	80.0	75.6	70.0	66.9
Subject-6	86.7	84.7	68.3	70.2
Mean±SD	80.2±6.5	78.7±6.0	74.4±7.4	74.1±7.1

Table II shows the optimized RQA parameters and response window optimization results for both μ and β-bands along with the median of selected number of nonlinear features across 5-fold cross-validation runs for each subject.

Fig. 1 illustrates the discriminative ability of the nonlinear features by comparing their frequency of selection in the optimized classification performance across all subjects and all folds. As shown, the LMAX and VMAX are the features with the highest frequency of selection across all subjects.

IV. DISCUSSION

In the present work, we evaluated the performance of a new set of graph-based RQA features for MI-BCI binary MI vs. Rest classification. Rooted in chaos theory, and the literature of nonlinear system dynamics, by characterizing the nonlinear recurrence patterns in μ and β spectral bands in phase space through graph-based RQA and complex network theory, these features introduce a new informative dimension to the analysis of EEG-based MI neural responses. Our findings demonstrated the feasibility of nonlinear graph-based RQA features for MI-BCI systems achieving a higher average accuracy (~80%) when compared to conventional linear spectral features (~74%). Our study investigated the performance of various RQA features. RR, DET, LMAX, LAM, VMAX, and RTE can all be indicative measures of the complexity of the neural system's dynamics. DET is a relative measure of the system's predictability and regularity (i.e., state of relative order). LMAX is an important measure of system's complexity as it is inversely related to the most positive Lyapunov exponent, which is a key indicator of chaos [12], RTE is also a measure of system's complexity as it is related to the Kolmogorov-Sinai entropy [23]. LAM and VMAX are analogous to DET and LMAX. However they are more pronounced for chaos-chaos transitions and were successfully applied to EEG data along with DET in [6] to

TABLE II. RECURRECE QUANTIFICATION ANALYSIS PARAMETER OPTIMIZATIPON

| Participant No.	Optimized μ-neighborhood threshold (ε)	Optimized β-neighborhood threshold (ε)	μ-time delay (τ)	β-time delay (τ)	μ- & β-embedding dimension (m)	# Selected features (median)	Optimized μ – response window	Optimized β – response window
Subject-1	0.07±0.02	0.05±0.02	6.0±0.0	3.0±0.5	4	29	6.4±3.5	4.4±1.3
Subject-2	0.07±0.03	0.07±0.04	6.0±0.0	3.0±0.0	4	20	10.0±0.0	10.0±0.0
Subject-3	0.05±0.03	0.06±0.02	6.0±0.0	3.0±0.0	4	26	10.0±0.0	9.0±2.2
Subject-4	0.07±0.03	0.03±0.01	6.0±0.0	3.0±0.4	4	12	10.0±0.0	9.0±2.2
Subject-5	0.06±0.02	0.06±0.03	6.0±0.3	3.0±0.1	4	14	9.0±2.2	6.4±3.5
Subject-6	0.05±0.01	0.05±0.01	7.0±0.0	4.0±0.0	4	12	8.0±2.7	8.0±2.7
Mean±SD	0.06±0.01	0.05±0.01	6.2±0.4	3.2±0.4	4.0±0.0	18.8±7.4	8.9±1.5	7.8±2.1
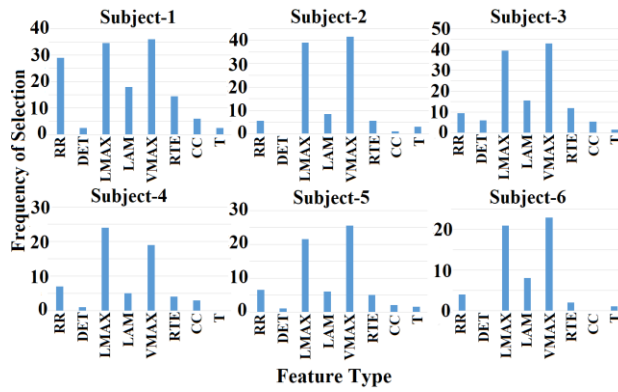
Figure 1. Selection frequency of the nonlinear RQA and graph-based features in the selected feature sets across all folds for each subject.

discriminate single trial event-related potentials. These features quantify transitions in the recurrence structures in phase space and provide a measure of complexity of the underlying nonlinear dynamics [16]; hence, they were successfully used to discriminate between MI and Rest tasks in our study. Our results provide evidence that these features can potentially add valuable information to conventional MI-BCI studies. DET and RTE features were found sensitive to MI neural responses similar to ME as proposed in [7]. However, other features such as LMAX, VMAX, LAM, and RR were more frequently selected across subjects and cross-validation folds. Our results also suggested that the topological aspect of the recurrence structures, reflected in CC and T, is valuable for the classification performance.

Future works need to further support our interpretations of the proposed nonlinear features as a new informative dimension for enhancing the BCI performance by validating nonlinearity in the dataset using a surrogate procedure. In addition, conducting a proper statistical evaluation of the proposed nonlinear features, as well as investigating other variations of graph-based nonlinear dynamics. Exploring powerful feature selection and classification algorithms should also be considered to extract robust discriminative patterns from a high dimensional nonlinear data.

V. Conclusion

This study focused on the evaluation RQA and graph-based features for a binary MI-BCI classification task. The performance evaluation revealed an average improvement of 5.8% as compared with the classical linear features. Optimized classification performance was achieved across both μ and β frequency bands and for various response window lengths ranging from 4.4-sec to 10-sec across subjects. Our results showed that the proposed nonlinear features can potentially enrich MI-BCI performance by exploiting the nonlinear neural dynamics embedded in MI neural responses beyond the classical linear spectral characteristics. These results suggest that nonlinear features can add a valuable dimension to the analysis of EEG signals for the improvement of MI-BCI system performance.

VI. acknowledgment

References

[1] N. Padfield, J. Zabalza, H. Zhao, V. Masero, and J. Ren, "EEG-based brain-computer interfaces using motor-imagery: Techniques and challenges," Sensors (Switzerland), 2019.

[2] S. M. Hosni, R. J. Deligani, A. Zisk, J. McLinden, S. B. Borghei, and Y. Shahriari, "An exploration of neural dynamics of motor imagery for people with amyotrophic lateral sclerosis," in Journal of Neural Engineering, 2020.

[3] G. Pfurtscheller, C. Neuper, and G. P. C. Neuper, "Motor imagery activates primary sensorimotor area in humans. - Abstract - Europe PubMed Central," Neurosci. Lett., 1997.

[4] S. Aggarwal and N. Chugh, "Signal processing techniques for motor imagery brain computer interface: A review," Array, 2019.

[5] T. Kasahara, K. Terasaki, Y. Ogawa, J. Ushiba, H. Aramaki, and Y. Masakado, "The correlation between motor impairments and event-related desynchronization during motor imagery in ALS patients," BMC Neurosci., 2012.

[6] N. Marwan and A. Meinke, "Extended recurrence plot analysis and its application to ERP data," in International Journal of Bifurcation and Chaos in Sciences and Engineering, 2004.

[7] E. Pitsik, N. Frolov, K. Hauke Kraemer, V. Grubov, V. Maksimenko, J. Kurths, and A. Hramov, "Motor execution reduces EEG signals complexity: Recurrence quantification analysis study," Chaos, 2020.

[8] G. Schalk, D. J. McFarland, T. Hinterberger, N. Birbaumer, and J. R. Wolpaw, "BCI2000: A general-purpose brain-computer interface (BCI) system," IEEE Trans. Biomed. Eng., 2004.

[9] D. J. McFarland, L. M. McCane, S. V. David, and J. R. Wolpaw, "Spatial filter selection for EEG-based communication," Electroencephalogr. Clin. Neurophysiol., 1997.

[10] C. Brunner, A. Delorme, and S. Makeig, "Eeglab – an Open Source Matlab Toolbox for Electrophysiological Research," Biomed. Eng. / Biomed. Tech., 2013.

[11] A. Kübler, F. Nijboer, J. Mellinger, T. M. Vaughan, H. Pawelzik, G. Schalk, D. J. McFarland, N. Birbaumer, and J. R. Wolpaw, "Patients with ALS can use sensorimotor rhythms to operate a brain-computer interface," Neurology, 2005.

[12] N. Marwan, et al. "Recurrence plots for the analysis of complex systems," Physics Reports. 2007.

[13] F. Takens, "Detecting strange attractors in turbulence," 1981.

[14] J. P. Eckmann, O. Oliffson Kamphorst, and D. Ruelle, "Recurrence plots of dynamical systems," EPL, 1987.

[15] M. Javorka, et al. "The effect of orthostasis on recurrence quantification analysis of heart rate and blood pressure dynamics," Physiol. Meas., 2009.

[16] C. L. Webber, Jr. and N. Marwan, "Recurrence Quantification Analysis -- Theory and Best Practices," in Springer series: Understanding Complex Systems. Springer International Publishing, Cham Switzerland., 2015.

[17] R. V. Donner, M. Small, J. F. Donges, N. Marwan, Y. Zou, R. Xiang, and J. Kurths, "Recurrence-based time series analysis by means of complex network methods," International Journal of Bifurcation and Chaos. 2011.

[18] R. V. Donner, Y. Zou, J. F. Donges, N. Marwan, and J. Kurths, "Recurrence networks-a novel paradigm for nonlinear time series analysis," New J. Phys., 2010.

[19] N. Marwan, J. F. Donges, Y. Zou, R. V. Donner, and J. Kurths, "Complex network approach for recurrence analysis of time series," Phys. Lett. Sect. A Gen. At. Solid State Phys., 2009.

[20] J. H. Feldhoff, et al. "Geometric signature of complex synchronisation scenarios," EPL, 2013.

[21] J. Foussier, P. Fonseca, X. Long, and S. Leonhardt, "Automatic feature selection for sleep/wake classification with small data sets," Bioinforma. 2013 - Proc. Int. Conf. Bioinforma. Model. Methods Algorithms, no. 2013, pp. 178–184, 2013.

[22] J. Rolink, P. Fonseca, X. Long, and S. Leonhardt, "Improving sleep/wake classification with recurrence quantification analysis features," Biomed. Signal Process. Control, 2019.

[23] M. S. Baptista, et al., "Kolmogorov-Sinai entropy from recurrence times," Phys. Lett. Sect. A Gen. At. Solid State Phys., 2010.